Available online at www.sciencedirect.com

ScienceDirect

Procedia Engineering 116 (2015) 103 – 110

Procedia Engineering

www.elsevier.com/locate/procedia

8th International Conference on Asian and Pacific Coasts (APAC 2015)

The Field of Flow Structures Generated by a Wave of Viscous Fluid Around Vertical Circular Cylinder Piercing the Free Surface

Giancarlo Alfonsi[a,*], Agostino Lauria[a], Leonardo Primavera[a]

[a]*Fluid Dynamics Laboratory, Università della Calabria, Via P. Bucci 42b, 87036 Rende (Cosenza), Italy*

Abstract

The diffraction of water waves induced by a large-diameter, surface-piercing, vertical circular cylinder is studied numerically. The Navier-Stokes equations in primitive variables are considered for the simulation of a given wave case, and the technique is followed of the Direct Numerical Simulation (DNS). The criterion of the imaginary part of the complex-eigenvalue pair of the velocity-gradient tensor for the extraction of the flow vortical structures is applied to the computed fields, so unveiling a complex configuration of structures at the free surface, and at the cylinder external walls. The most energetic modes of the flow are further extracted from the DNS-simulated fields by using the Karhunen-Loève decomposition (KL). A "reduced" velocity field is reconstructed using the first three most energetic eigenfunctions of the decomposition, and its evolution is followed through a sequence of time steps.

Peer- Review under responsibility of organizing committee , IIT Madras , and International Steering Committee of APAC 2015

Keywords: Wave diffraction; Vertical circular cylinder; Navier-Stokes equations; Direct Numerical Simulation; Vortical structures

1. Introduction

The diffraction of small-amplitude water waves impinging large bodies has been studied by several authors with different techniques (see also Alfonsi et al. 2012*a* and references therein), though being (besides experiments) the numerical integration of the full Navier-Stokes equations the only rigorous, physically-consistent approach to be

* Corresponding author. Tel.: +39-0984-49-6571; fax: +39-0984-49-6578.
E-mail address: giancarlo.alfonsi@unical.it

Peer- Review under responsibility of organizing committee , IIT Madras , and International Steering Committee of APAC 2015
doi:10.1016/j.proeng.2015.08.270

followed, in order to obtain a flow field that correctly represents the numerical equivalent of the physical phenomenon at hand. In the present work, the three-dimensional, time-dependent full Navier-Stokes equations in primitive variables are considered for the numerical simulation of a case of water wave impinging on a large-diameter, surface-piercing, vertical circular cylinder (the Keulegan-Carpenter number is KC = 0.578, the field Reynolds number is Re = 1862), and the DNS approach is followed in the simulations (no models for the fluctuating portion of the velocity field are used in the calculations, see, among others, Alfonsi 2011). The swirling-strength criterion, as devised by Zhou et al. (1999) for flow-structure extraction, is applied to the computed fields, so unveiling a complex configuration of viscous-flow structures both at the free surface, and at the cylinder external wall, under the free surface. The technique of the Karhunen-Loève decomposition (KL) is further applied to the DNS-simulated velocity fields for the extraction of the most energetic modes of the flow. A "reduced" velocity field is then reconstructed, based on a limited number of the most energetic modes of the flow (three in particular), and its spatial configuration and evolution in time is illustrated mainly in terms of isosurfaces of the fluid velocity component (u) in the direction of the oncoming wave (x).

2. Numerical Simulations

The system of the three-dimensional, nondimensional, time-dependent Navier-Stokes equations in primitive variables with body forces, are considered for the case at hand (the fluid is incompressible and viscous, Einstein summation convention applies to repeated indexes, *i=1,2,3*):

$$\frac{\partial u_i}{\partial t} + u_j \frac{\partial u_i}{\partial x_j} = -\frac{\partial p}{\partial x_i} + \frac{1}{\mathrm{Re}_{NS}} \frac{\partial^2 u_i}{\partial x_j \partial x_j} + \delta_{i,3} \ , \qquad \frac{\partial u_i}{\partial x_i} = 0 \tag{1}$$

where $u_i(u,v,w)$ are the velocity components along $x_i(x,y,z)$, p is the pressure, and δ_{ij} is the Kronecker delta. Variables and operators are nondimensionalized by the cylinder diameter D for lengths, by the group $\sqrt{Dg}$ for velocities, by ρDg for pressures, and by $\sqrt{D/g}$ for time, where Re_{NS} is the Reynolds number resulting from the nondimensionalization procedures (see also at Table 1). For the execution of the calculations, a finite-volume computational code, and a specially-assembled multicore computing system, have been used, the latter including 2 Intel Xeon 5660 exa-core processors (a total of 12 available CPU), a maximum of 48 GB of RAM, and up to 1.8 TB of mass memory (for further details on the numerical simulations one can refer to Alfonsi et al. 2012*b*). In the numerical simulations of present work, no models for the fluctuating portion of the velocity field have been used, so that the Navier-Stokes equations are solved following the technique of the Direct Numerical Simulation (DNS).

Table 1. Characteristic parameters of the numerical simulations (KC = 0.578, Re = 1862)

Computing domain (D units) (L is wave length, d is still-water level)		
$L_x(=2L)=7.8$	$L_y(=2L)=7.8$	$L_z(=3d)=3.0$
Computational grid (D units) (N_{tot} = 18,669,960 total number of grid points used)		
Blocks 1-5	$-3.9 < x < 3.9$	$-3.9 < y < 3.9$ $\quad -2 < z < 1.0$
Space and time resolutions (η and τ_η units)		
$\Delta x_{cylinder\_wall} = 0.45\eta$	$\Delta x_{end\_of\_block\_3} = 2.25\eta$	$\Delta x_{blocks\_1,5} = 2.25\eta$
$\Delta y_{cylinder\_wall} = 0.45\eta$	$\Delta y_{end\_of\_block\_3} = 2.25\eta$	$\Delta y_{blocks\_2,4} = 2.25\eta$
$\Delta z_{blocks\_1,2,3,4,5} = 1.70\eta$	$\Delta t = 0.002\tau_\eta$	

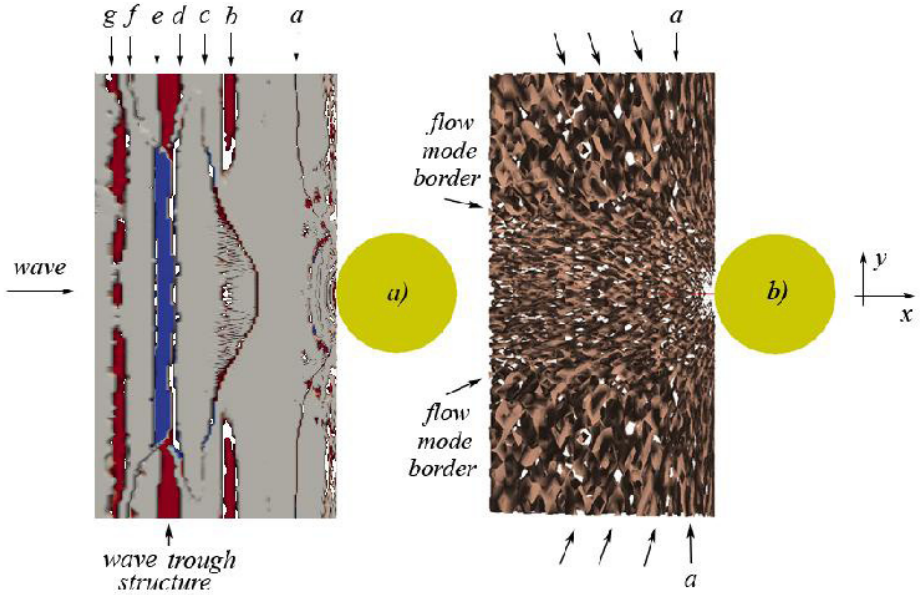

Fig. 1. Flow-field representation at T=0.144, top view (free surface): *a)* flow structures as extracted with the swirling-strength criterion; *b)* surfaces of constant x-velocity from reconstruction based on the three most energetic KL eigenfunctions (T is wave period).

With concern to the smallest-scale-resolution requirements in DNS calculations, the criterion is usually followed of resolving the Kolmogorov space and time microscales:

$$\eta = \left(\frac{\nu^3}{\bar{\varepsilon}}\right)^{1/4}, \quad \tau_\eta = \left(\frac{\nu}{\bar{\varepsilon}}\right)^{1/2} \tag{2}$$

or, at most, limited multiples of the latter. As concerns the procedure for the evaluation of the Kolmogorov microscales (2), they can be evaluated by estimating the average rate of dissipation of kinetic energy per unit mass ($\bar{\varepsilon}$), as obtained from some mean-flow quantities (Bakewell and Lumley 1967). For the wave case of present work, one obtains:

$$\bar{\varepsilon} \cong 0.00000525\ D^{1/2} g^{3/2}, \quad \eta = 0.0147\ D, \quad \tau_\eta = 3.45\sqrt{D/g} \tag{3}$$

The computing domain has been discretized in a multiblock, 5-block computational grid (Table 1). With the grid-point configuration used, the space resolutions Δx and Δy at the cylinder wall are able to resolve less than one half of the Kolmogorov spatial microscale while at the domain external boundaries they are still able to resolve less than two and a half η. These values are perfectly in the ranges usually adopted in DNS (Alfonsi 2011).

3. Flow-Structure Extraction

Of the existing techniques for the extraction of a flow vortical structures (see, among others, Alfonsi 2006), the criterion of the imaginary part of the complex eigenvalue pair of the velocity-gradient tensor (the swirling-strength criterion) as devised by Zhou et. al. (1999), has been adopted. By considering the system of the flow governing equations, an arbitrary point O can be chosen in the field, and a Taylor-series expansion of each velocity component can be performed in terms of space coordinates with the origin in O, so that the first-order pointwise linear approximation at that point becomes:

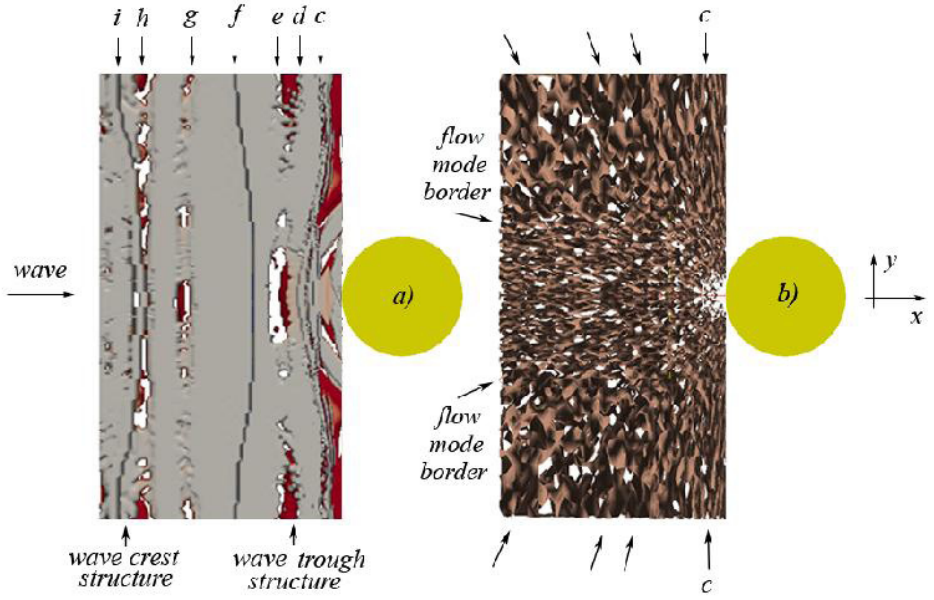

Fig. 2. Flow-field representation at T=0.5, top view (free surface): *a)* flow structures as extracted with the swirling-strength criterion; *b)* surfaces of constant x-velocity from reconstruction based on the three most energetic KL eigenfunctions (T is wave period).

$$u_i = A_i + A_{ij} x_j \tag{4}$$

($A_{ij} = \partial u_i / \partial x_j$ is the velocity-gradient tensor). If O is located at a critical point, the zero-order terms are zero. In the case of incompressible flow, the characteristic equation of A_{ij}, and its discriminant, assume the form:

$$\lambda^3 + Q\lambda + R = 0; \qquad Dsc = \left(R^2/4\right) + \left(Q^3/27\right) \tag{5}$$

(Q and R are scalar invariants of the velocity-gradient tensor). When $Dsc > 0$, the velocity-gradient tensor has one real eigenvalue and a pair of complex-conjugate eigenvalues. Zhou et al. (1999) adopted the criterion of identifying vortices by visualizing isosurfaces of prescribed values of the imaginary part of the complex-eigenvalue pair of the velocity-gradient tensor (the swirling-strength parameter). The swirling strength represents a measure of the local swirling rate inside a vortical structure, so that isosurfaces of the imaginary part of the complex eigenvalue pair of the velocity-gradient tensor can be used to visualize vortices. The method is frame independent and, due to the fact that the eigenvalue is complex only in regions of local circular or spiralling streamlines, it automatically eliminates regions having no local spiralling motion (see, among others, Alfonsi and Primavera 2007*a*, 2008, 2009*a,b*, Alfonsi et al. 2011, 2012*c,d*).

4. Karhunen-Loève Decomposition

Within the group of the Proper Orthogonal Decomposition methods, a powerful technique for the extraction of the most energetic modes of a flow, is the Karhunen-Loève (KL) decomposition (among others, Lumley 1971, Sirovich 1987). By considering an ensemble of temporal realizations of a non-homogeneous, square integrable, three-dimensional velocity field on a finite domain, one wants to find the most similar function to the elements of the ensemble on average. This corresponds to find a deterministic vector function that maximizes the normalized inner product of the candidate structure with the field. A necessary condition for this problem is that the vector function $\phi_i(x_j)$ is an eigenfunction, solution of the eigenvalue problem and first-kind Fredholm integral equation:

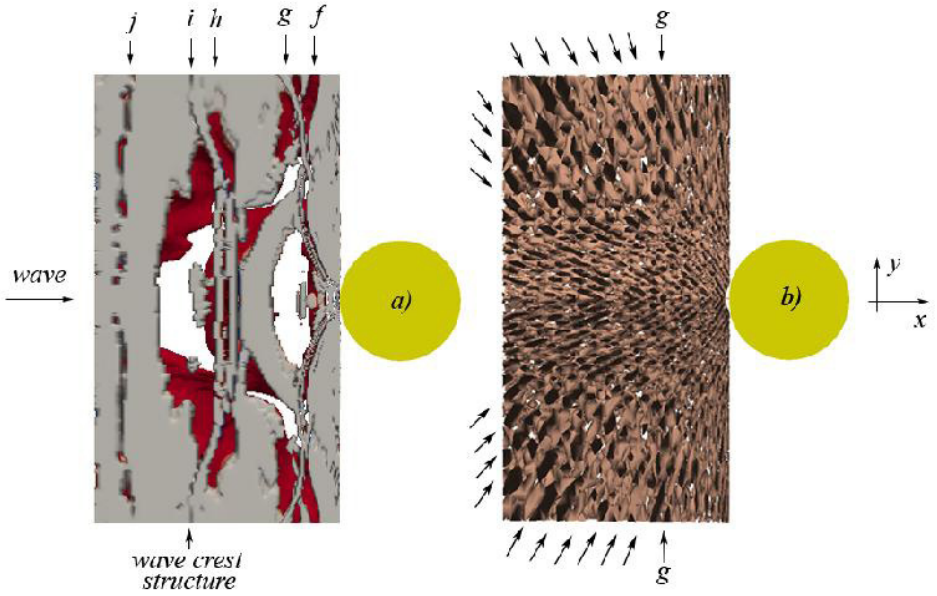

Fig. 3. Flow-field representation at T=0.75, top view (free surface): *a)* flow structures as extracted with the swirling-strength criterion; *b)* surfaces of constant x-velocity from reconstruction based on the three most energetic KL eigenfunctions (T is wave period).

$$\int_{\Lambda} R_{ij}(x_l, x_l')\varphi_j(x_l')dx_l' = \int_{\Lambda} \langle u_i(x_k, t)u_j(x_k', t)\rangle \varphi_j(x_k')dx_k' = \lambda\varphi_i(x_k) \tag{6}$$

[$R_{ij} = \langle u_i(x_l, t)u_j(x_k', t)\rangle$ is the two-point velocity correlation tensor, $(i, j, l, k = 1,2,3)$], where the maximum $\phi_i(x_j)$ corresponds to the largest eigenvalue λ of (6). When the domain is bounded, there exists a denumerable infinity of solutions of (6) (Hilbert-Schmidt theory), and these solutions [$\phi_i^{(n)}(x_j)$] are called the empirical eigenfunctions. To each eigenfunction is associated a real, positive eigenvalue, and the eigenfunctions form a complete set. Every member of the ensemble can be reconstructed by means of a modal decomposition in the eigenfunctions themselves, that can be seen as a decomposition of the originary random field into deterministic structures with random, time-dependent coefficients. The modal amplitudes are uncorrelated, and their mean square values are the eigenvalues themselves (see, among others, Carbone et al. 2002, Alfonsi et al. 2003*a,b*, Alfonsi and Primavera 2002, 2005*a*, 2006, 2007*b*, Vecchio et al. 2005). In the context of the problem at hand here, the high-performance computational code for the execution of KL calculations has been used, as originally developed by Alfonsi and Primavera (2005*b*, 2007*c*). The code is general, and can be used in all kind of problems, directly in physical space. More in particular, the two-point velocity-correlation tensor is calculated in its complete form, so that the optimal representation of the velocity field outlined above is calculated in all the three directions x,y,z. The integral in equation (6) is evaluated numerically by using the weight functions of the trapezoidal rule.

5. Results

As concerns flow structures, the results have been reported by visualizing structures corresponding to a given value of the swirling-strength parameter. The external surfaces of the structures are colored with the spanwise (y) component of the vorticity in a blue-to-red scale (blueish = negative y-vorticity, reddish = positive y-vorticity). As concerns the KL decomposition, as a result of the procedure, a total of 117,600 eigenfunctions and corresponding eigenvalues have been calculated in a computing subdomain located immediately upstream from the cylindrical body. It has been verified that the first three resulting eigenfunctions of the decomposition alone, exhibit a cumulative energy content of more than 99.8% of the total kinetic energy of the original field. On this basis, a

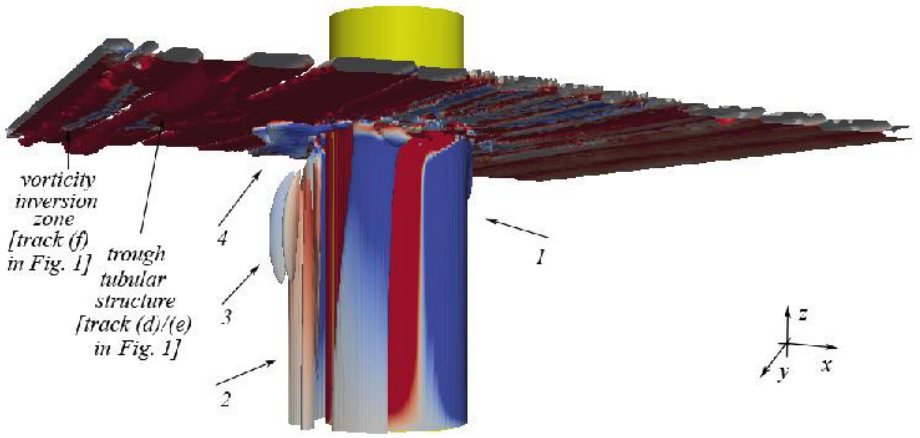

Fig. 4. Flow-field representation at T=0.144 (under the free surface): quasi-side view of flow structures (swirling-strength criterion).

"reduced" velocity field has been reconstructed, by taking into account only the three most energetic eigenfunctions of the KL decomposition. The time series of the KL flow fields is represented in terms surfaces of constant x-fluid velocity (u).

In Figure 1*a,b* the free-surface fields at $T = 0.144$ are represented. Figure 1*a* shows that a considerable portion of the free surface is still irrotational. Upstream from the cylinder, track (*a*) denotes the descending portion of the wave, track (*b*) is interrupted by track (*c*), track (*d*)/(*e*) denotes the presence of the wave trough, while track (*f*) mirrors the vorticity-inversion phenomenon in front of the cylinder (Alfonsi et al. 2012*b*). What happens there is that the presence of the cylindrical body in front of the descending portion of the wave, determines an inversion of the fluid-particle orbital paths, with the consequence that the shear-stress field induces a strong negative vorticity field (blueish) in the zone right in front of the cylinder. An inspection to Figure 1*b* shows that the only detectable similarity between the visualizations of Figure 1*a* and 1*b* is the position of track (*a*) (also shown in Figure 1*b*). Further upstream from track (*a*) in Figure 1*b*, other tracks are present (oblique arrows), representing borders between flow structures with high kinetic-energy content. The field upstream from the cylinder is actually divided in two zones, a first zone characterized by small flow scales, and a second zone characterized by larger flow scales. The flow-mode border track is shown in Figure 1*b*, between the two zones of high-energy scale-organization.

In Figure 2*a,b* the free-surface fields at $T = 0.5$ are shown. Figure 2*a* shows the evolution of the diffraction tracks with respect to the previous instant. On the upstream side of the cylinder, track (*d*)/(*e*) has in practice collapsed into a unique structure, tracks (*f*) and (*g*) denote the wave ascending portion, and track (*h*)/(*i*) indicates the presence of a new crest in the domain. Again, the only detectable similarity between the visualizations of Figure 2*a* and 2*b*, is the position of track (*c*), while further upstream from track (*c*) in Figure 3*b*, other tracks are again present (oblique arrows), representing borders between flow structures with high kinetic-energy content. An inspection to Figure 2*b* shows that the field upstream from the cylinder is again divided in two zones, a first small-scale zone, and a second large-scale zone. The flow-mode border track is again shown in Figure 2*b*.

In Figure 3*a,b* the free-surface fields at $T = 0.75$ are represented. In Figure 3*a*, track (*g*) mirrors the ongoing interaction between wave and cylinder, while the wave-crest track is approaching the cylinder, assuming, at the same time, a complex (*h*)/(*i*) track configuration in the center of the domain. Also in this case, the only similarity between the fields represented in Figure 3*a* and 3*b*, is track (*g*), while in Figure 3*b*, other tracks are present (oblique arrows), always representing borders between flow structures with high kinetic-energy content. Differently from the previous instants, it appears from Figure 3*b*, that no more discontinuities between smaller and larger high-kinetic-energy flow scales are present. The field of high-energy scales continuously evolves from the center to the periphery of the domain, forming a "harrow-tip" pattern.

In Figure 4 the fields under the free surface at $T = 0.144$ are represented. It can be noted that in Figure 4, the underwater portions of track (*f*) (the vorticity inversion tubular zone) and track (*d*)/(*e*) (the wave trough tubular structure) already depicted in Figure 1, are clearly detectable, both chracterized by high positive y-vorticity. At the

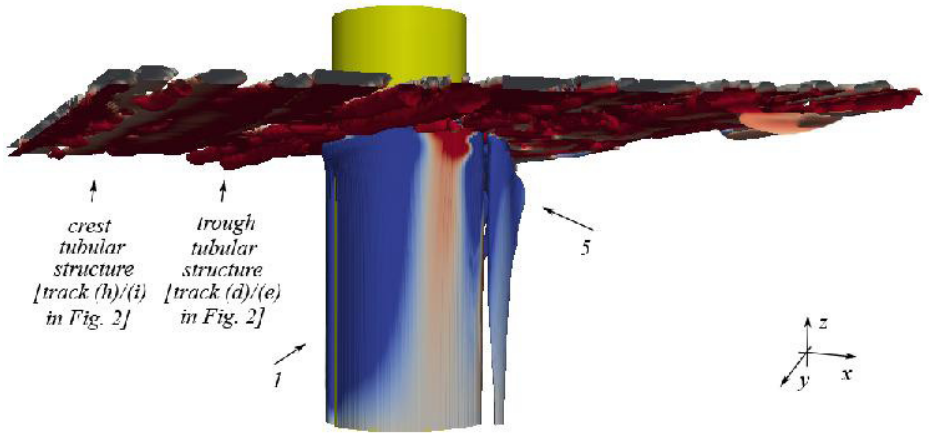

Fig. 5. Flow-field representation at T=0.5 (under the free surface): quasi-side view of flow structures (swirling-strength criterion).

cylinder wall, arrow 1 indicates a flow structure that completely encompasses the cylindrical body, with strong negative spanwise vorticity on the downstream- and upstream sides, and strong positive vorticity laterally. Arrows 2, 3, and 4 indicate a complex distribution of viscous-flow structures on the upstream side of the cylinder, directly related to the above-mentioned vorticity-inversion- and wave-trough tubular structure at the free surface. Structure 4 in particular represents the underwater counterpart of the phenomenon of accumulation of fluid mass upstream from the cylinder, that occurs when the wave approaches the cylindrical body.

In Figure 5 the fields under the free surface at $T = 0.5$ are represented. Also in this case, track (d)/(e) and track (h)/(i) (the wave crest tubular structure) already depicted in Figure 2, are clearly detectable. Note that track (d)/(e) now mirrors a double-tubular trough structure. At the cylinder wall, structures 2, 3 and 4 have practically disappeared, structure 1 has extended its negative-vorticity portion upstream from the cylinder, and a new vertically-elongated structure 5, with negative vorticity, has appeared downstream from the cylinderical body.

In Figure 6 the fields under the free surface at $T = 0.75$ are represented. Again, the track (h)/(i), already depicted in Figure 3, is detectable, as characterized by its high positive-vorticity content. At the cylinder wall, structures 1 and 5 are still present.

6. Concluding Remarks

The diffraction of water waves around large-diameter, surface-piercing, vertical circular cylinder, has been investigated by solving numerically the system of the Navier-Stokes equations. The application of the swirling strength criterion to the computed fields has unveiled the existence of a complex environment of vortical structures, both at the free surface, and under the free surface. The Karhunen-Loève decomposition of the fields has further shown that the relevant dynamics of the wave-cylinder interaction process can be caught by recostructing a reduced velocity field, only based on the three most energetic eigenfunctions of the decomposition.

References

Alfonsi, G., 2006. Coherent structures of turbulence: methods of eduction and results. Applied Mechanics Reviews 59, 307-323.

Alfonsi, G., 2011. On direct numerical simulation of turbulent flows. Applied Mechanics Reviews 64, Art. 020802.

Alfonsi, G., Ciliberti, S.A., Mancini, M., Primavera, L., 2011. Hairpin vortices in turbulent channel flow. Procedia Computer Science 4, Elsevier Science, Amsterdam New-York, pp. 801-810.

Alfonsi, G., Lauria, A., Primavera, L., 2012*a*. Flow structures around a large-diameter circular cylinder. Journal of Flow Visualization and Image Processing 19, 15-35.

Alfonsi, G., Lauria, A., Primavera, L., 2012*b*. Structures of a viscous-wave flow around a large-diameter circular cylinder. Journal of Flow Visualization and Image Processing 19, 323-354.

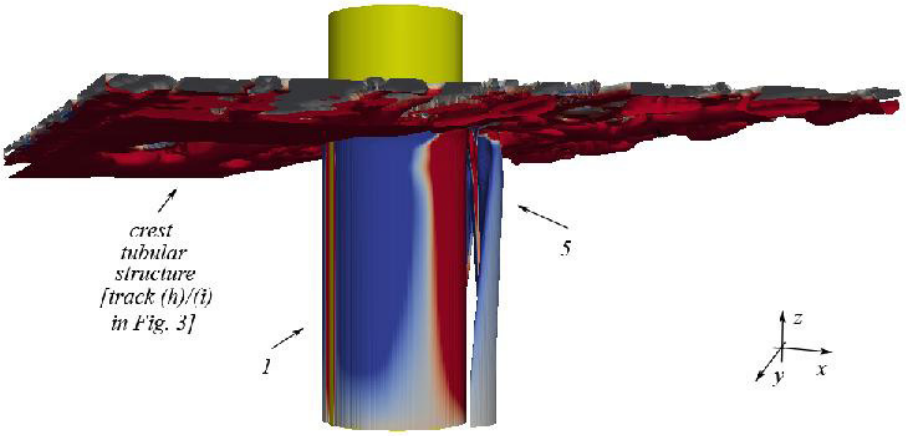

Fig. 6. Flow-field representation at T=0.75 (under the free surface): quasi-side view of flow structures (swirling-strength criterion).

Alfonsi, G., Lauria, A., Primavera, L., 2012*c*. A study of vortical structures past the lower portion of the Ahmed car model. Journal of Flow Visualization and Image Processing 19, 81-95.

Alfonsi, G., Ciliberti, S.A., Mancini, M., Primavera, L., 2012*d*. Turbulent events in a wall-bounded turbulent flow. Journal of Flow Visualization and Image Processing 19, 139-160.

Alfonsi, G., Primavera, L., 2002. Coherent structure dynamics in turbulent channel flow. Journal of Flow Visualization and Image Processing 9, 89-98.

Alfonsi, G., Primavera, L., 2005*a*. Description of turbulent events through the analysis of POD modes in numerically simulated turbulent channel flow. Lecture Notes in Computer Science 3514, Springer Verlag, Berlin Heidelberg, pp. 623-630.

Alfonsi, G., Primavera, L., 2005*b*. A parallel computational code for the eduction of coherent structures in fluid dynamics. Lecture Notes in Computer Science 3606, Springer Verlag, Berlin Heidelberg, pp. 381-392.

Alfonsi, G., Primavera, L., 2006. Dynamics of POD modes in wall-bounded turbulent flow. Lecture Notes in Computer Science 3991, Springer Verlag, Berlin Heidelberg, pp. 465-472.

Alfonsi, G., Primavera, L., 2007*a*. Vortex identification in the wall region of turbulent channel flow. Lecture Notes in Computer Science 4487, Springer Verlag, Berlin Heidelberg, pp. 9-16.

Alfonsi, G., Primavera, L., 2007*b*. The structure of turbulent boundary layers in the wall region of plane channel flow. Proceedings of the Royal Society A 463, 593-612.

Alfonsi, G., Primavera, L., 2007*c*. A parallel computational code for the Proper Orthogonal decomposition of turbulent flows. Journal of Flow Visualization and Image Processing 14, 267-286.

Alfonsi, G., Primavera, L., 2008. On identification of vortical structures in turbulent shear flow. Journal of Flow Visualization and Image Processing 15, 201-216.

Alfonsi, G., Primavera, L., 2009*a*. Determination of the threshold value of the quantity chosen for vortex representation in turbulent flow. Journal of Flow Visualization and Image Processing 16, 41-49.

Alfonsi, G., Primavera, L., 2009*b*. Temporal evolution of vortical structures in the wall region of turbulent channel flow. Flow Turbulence and Combustion 83, 61-79.

Alfonsi, G., Primavera, L., Felisari, R., 2003*a*. On the behavior of POD modes of the flow past a perforated plate. Journal of Flow Visualization and Image Processing 10, 105-117.

Alfonsi, G., Restano, C., Primavera, L., 2003*b*. Coherent structures of the flow around a surface-mounted cubic obstacle in turbulent channel flow. Journal of Wind Engineering and Industrial Aerodynamics 91, 495-511.

Bakewell, H.P., Lumley, J.L., 1967. Viscous sublayer and adjacent wall region in turbulent pipe flow. Physics of Fluids 10, 1880-1889.

Carbone, V., Lepreti, F., Primavera, L., Pietropaolo, E., Berrilli, F., Consolini, G., Alfonsi, G., Bavassano. B., Bruno, R., Vecchio, A., Veltri, P., 2002. An analysis of the vertical photospheric velocity field as observed by THEMIS. Astronomy and Astrophysics 381, 265-270.

Lumley, J.L., 1971. Stochastic tools in turbulence. Academic Press, New-York.

Sirovich, L., 1987. Turbulence and the dynamics of coherent structures. Part 1: Coherent structures. Part 2: Symmetries and transformations. Part 3: Dynamics and scaling. Quarterly Applied Mathematics 45, 561-590.

Vecchio, A., Carbone, V., Lepreti, F., Primavera, L., Sorriso-Valvo, L., Veltri, P., Alfonsi, G., Straus, Th., 2005. Proper Orthogonal Decomposition of solar photospheric motions. Physical Review Letters 95, Art. 061102.

Zhou, J., Adrian, R.J., Balachandar, S., Kendall, T.M., 1999. Mechanisms for generating coherent packets of hairpin vortices in channel flow. Journal of Fluid Mechanics 387, 353-396.